Supporting Information

Optical introduction and manipulation of plasmon-exciton-trion coupling in a Si/WS_2/Au nanocavity

*Shimei Liu,[1#] Fu Deng,[2#] Weijie Zhuang,[1] Xiaobing He,[1] Hongxin Huang,[1] Jing-Dong Chen,[3] Huajian Pang,[1] and Sheng Lan[1]**

[1]Guangdong Provincial Key Laboratory of Nanophotonic Functional Materials and Devices, School of Information and Optoelectronic Science and Engineering, South China Normal University, Guangzhou 510006, China

[2]Department of Physics, The Hong Kong University of Science and Technology, Kowloon, Hong Kong, China

[3]College of Physics and Information Engineering, Minnan Normal University, Zhangzhou 363000, China

#These authors contributed equally to this work.

*Corresponding author: slan@scnu.edu.cn

Supplementary Note 1

Two-dimensional materials, such as WS_2 monolayer, are usually used in the study of plasmon-exciton coupling with a variety of nanocavities. All-metallic particle-on-film systems are the most commonly used nanocavities because significantly enhanced electric field can be achieved. However, the large imaginary part of metals leads to pronounced temperature rise in such nanocavities, which may lead to the damage of the two-dimensional materials. For this reason, much attention has been paid to dielectric-metal hybrid nanocavities, such as Si/Au nanocavities investigated. In Figure S1a,b, we show the temperature distributions in the XZ plane in a Au/Au and a Au/WS_2/Au nanocavity induced by the irradiation of a 488-nm laser beam with a power of P = 1.0 mW. It can be seen that the maximum temperature reaches T_{max} = 584 K for the Au/Au nanocavity. The insertion of a WS_2 monolayer leads to the increase of maximum temperature to T_{max} = 669 K. For comparison, we present the temperature distributions calculated for a Si/Au and a Si/WS_2/Au nanocavity under the same condition. It was found that the maximum temperature in the Si/Au nanocavity is dramatically reduced to T_{max} = 446 K. In addition, the addition of the WS_2 monolayer results in only a slight increase in T_{max} (457 K). Here, the thermal conductivity and heat capacity of WS_2 monolayer used in the numerical simulations are 142 W m^{-1} K^{-1} and $6.03 \cdot 10^5$ J K^{-1}.[1, 2]

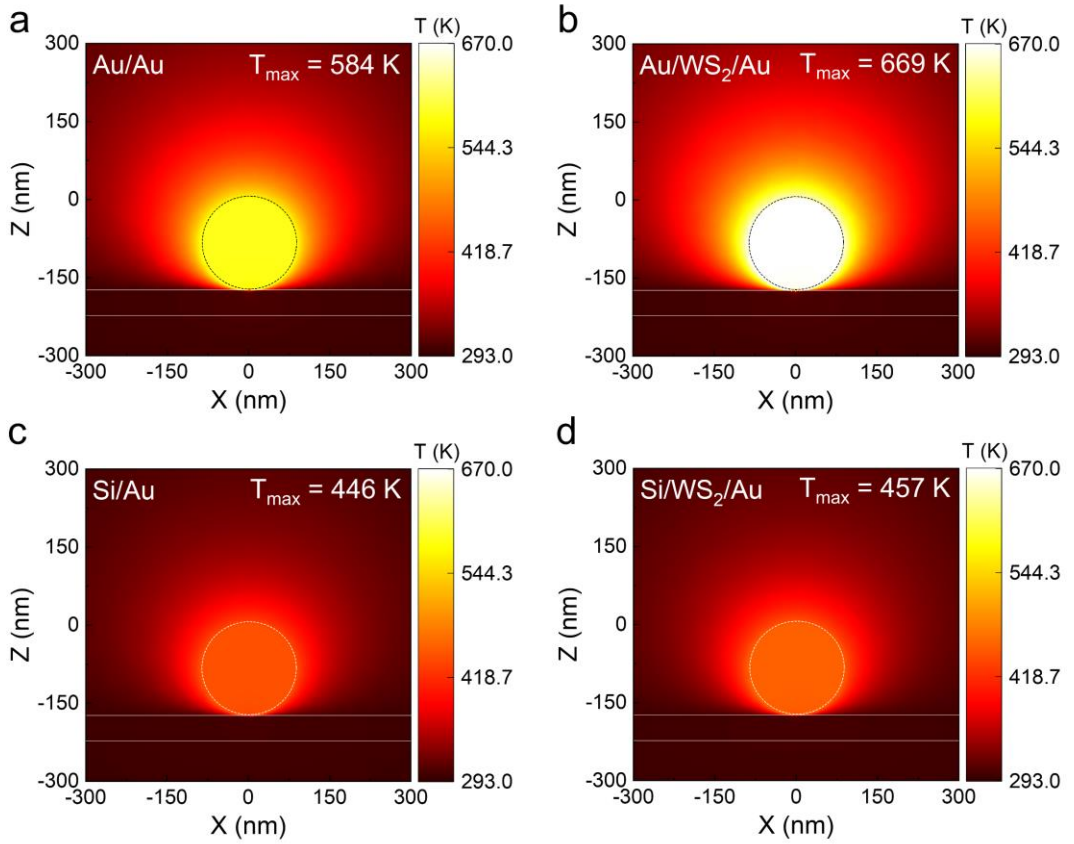

Figure S1. Temperature rises induced by a 488-nm laser beam of 1.0 mW in a Au/Au nanocavity (a), a Au/WS_2/Au nanocavity (b), a Si/Au nanocavity (c), and a Si/WS_2/Au nanocavity (d). The diameters of Au and Si nanoparticles are chosen to be 175 nm.

Supplementary Note 2

Basically, the plasmon-exciton coupling strength in a Si/WS_2/Au nanocavity can be expressed as follows:[3-5]

$$g = \mu_e \sqrt{\frac{\pi \hbar N c}{\lambda \varepsilon \varepsilon_0 V}}. \quad (1)$$

Here, V is the mode volume of the nanocavity, which can be written as:[6]

$$V = \frac{\int \varepsilon(\vec{r}) \left|\vec{E}(\vec{r})\right|^2 d^3\vec{r}}{\max(\varepsilon(\vec{r}) \left|\vec{E}(\vec{r})\right|^2)}. \quad (2)$$

For a nanocavity with d = 174 nm (the diameter of the Si nanoparticle), the mode volume is calculated to be ~ 7.16×10^{-24} m^3. Based on the backward scattering spectrum simulated for the nanocavity, the coupling strength is estimated to be g = 32.5 meV.[7] Therefore, the number of excitons coupled to the nanocavity is derived to be N ~5.0 based on Eq. (1). The following parameters are used in the calculation, μ_e = 56D, $\varepsilon_{WS_2} \approx$ 28.6 $C^2/(N\cdot m^2)$, $\varepsilon_{Si} \approx$ 15.4 $C^2/(N\cdot m^2)$, $\varepsilon_{Au} \approx$ 0.21 $C^2/(N\cdot m^2)$.

Now we estimate the number of excitons and trions injected by the 488-nm laser light with a power of 1.00 mW. The number of photons carried by the laser light is calculated to be ~ 9.8×10^{14}. In our case, the diameter of the laser beam and the size of the hot spots are found to be 1.19 μm and 8.8 nm. Since the absorption of the WS_2 monolayer is ~15% and the lifetime of excitons is ~4.4 ns,[8, 9] the number of photons injected into the hot spots, which can be coupled into the nanocavity, is calculated to be N ~70. In this case, it is assumed that all the photons absorbed in the hot spots are converted to excitons.

Supplementary Note 3

We measured the PL spectra of Si/WS_2/Au nanocavities composed of Si nanoparticles with different diameters at different laser powers, as shown in Figure S2. The PL spectra of the nearby WS_2 monolayers obtained under the same excitation condition are also provided for comparison. In each case, the PL spectrum is decomposed into the contributions of excitons and trions. In this way, the intensities of excitons and trions and their resonant wavelengths at different laser powers can be extracted.

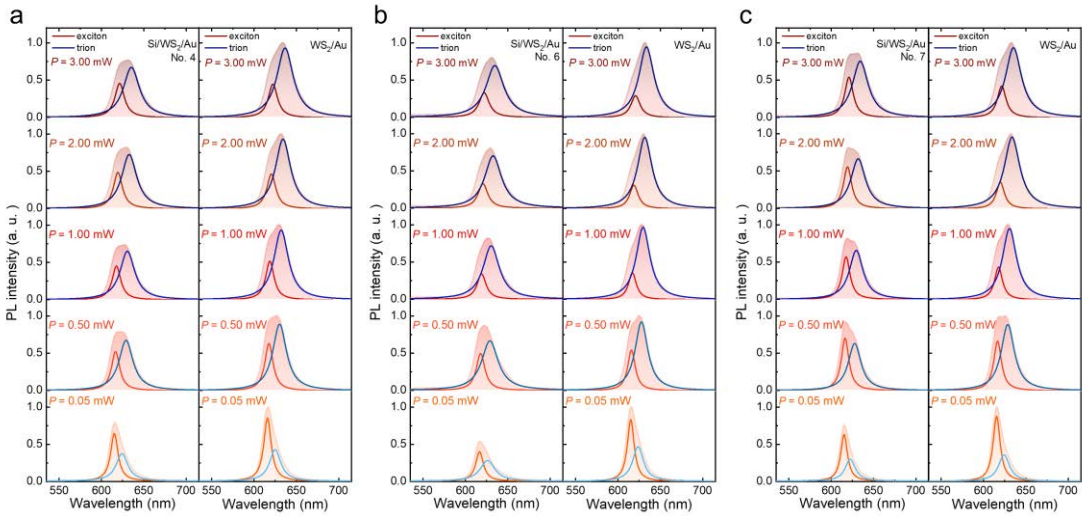

Figure S2. PL spectra measured for Si/WS_2/Au nanocavities constructed with Si nanoparticles of different diameters at different laser powers. The PL spectra of the nearby WS_2 monolayers measured under the same conditions are provided for comparison. In each case, the PL spectrum is decomposed into the contributions of excitons and trions possessing Lorentz lineshapes.

Supplementary Note 4

In Figure S3a,b, we present the dependences of the resonant wavelengths of excitons and trions on the laser power. It can be seen that both of them are shifted to longer wavelengths with increasing laser power. Meanwhile, a broadening of linewidth is observed for both excitons and trions when the laser power is increased, as shown in Figure S3c,d.

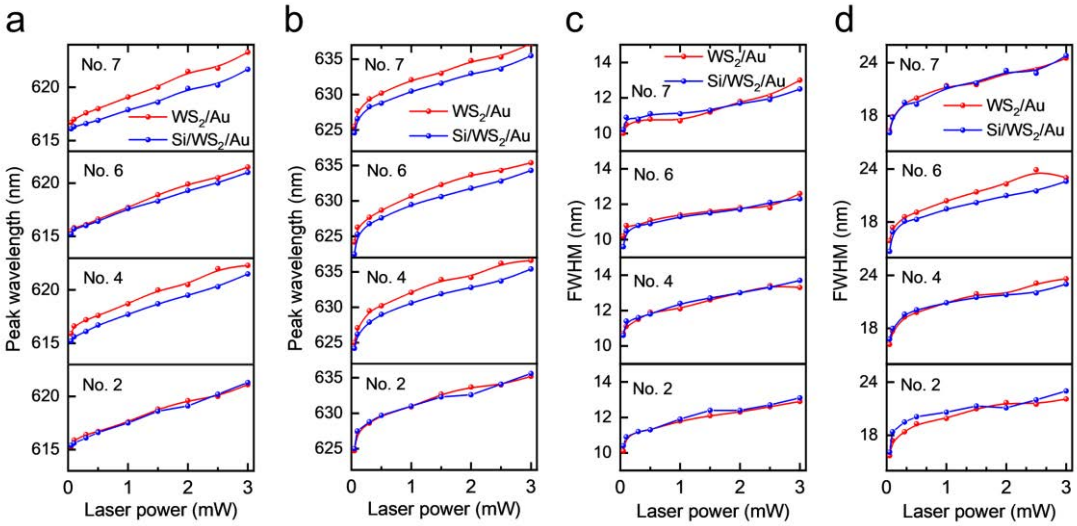

Figure S3. Dependences of the resonant wavelengths of excitons (a) and trions (b) on the laser power extracted from the decompositions of the PL spectra measured for different Si/WS_2/Au nanocavities. The corresponding dependences of the linewidths of excitons and trions on the laser power are shown in (c) and (d), respectively.

Supplementary Note 5

As discussed in the main text, we extracted from the PL spectra of the WS_2 monolayer only the wavelengths and linewidths of the excitons and trions. The oscillator strengths of the excitons and trions are extracted from the fitting of the scattering spectra of the Si/WS_2/Au nanocavity (see a typical example in Figure S8). In Table 1, we present the oscillator strengths of the excitons and trions extracted from the scattering spectra. For comparison, we also provide the emission intensities of the excitons and trions derived from the fitting of the PL spectra at different laser powers. In each case, it is noticed that the value of f_e/f_t is much different from that of I_e/I_t. It implies that the oscillator strength of the trions will be overestimated if we used the emission intensities of the excitons and trions as their oscillator strengths.

	P = 0.0 mW	P = 2.5 mW	P = 3.0 mW	P = 3.5 mW	P = 4.0 mW
f_e	0.5	1.00	1.30	1.50	1.70
f_t		0.85	1.20	1.30	1.45
f_e/f_t		1.18	1.08	1.15	1.17
I_e		1384	1695	2864	3220
I_t		4629	5438	8139	8486
I_e/I_t		0.299	0.312	0.352	0.379

Table 1. Oscillator strengths of the excitons and trions derived at different laser powers based on the fitting of the scattering spectra of a Si/WS_2/Au nanocavity. The emission intensities of the excitons and trions extracted from the fitting of the PL spectra are also provided for comparison.

Supplementary Note 6

Since the excitons in WS_2 monolayer oriented mainly in the xy plane, we first examined the distribution of the in-plane electric field intensity ($|E_{xy}/E_0|$) calculated for a Si/WS_2/Au nanocavity with d = 183 nm (No. 6), which is located at the scattering peak in the backward scattering spectrum, as shown in Figure S4a. In this case, the nanocavity was excited by using a plane wave polarized along the x direction. One can see two hot spots with enhanced electric field located symmetrically with respect to the y axis. It should be emphasized that the size of the hot spots is much smaller than that of the laser spot. Therefore, the enhancement or reduction in the PL intensity of the WS_2 monolayer in the presence of a Si nanoparticle may not be significant as expected from the enhancement factor (~35) of the electric field intensity. In Figure S4b, we present the two-dimensional scattering spectra calculated for Si/WS_2/Au nanocavities composed of Si nanoparticles with different diameters. One can identify a scattering dip originating from the plasmon-exciton coupling. We also examined the wavelength-dependent enhancement factors of the in-plane electric field (i.e., $|E_{xy}/E_0|^2$), which governs the plasmon-exciton coupling, achieved in Si/Au nanocavities formed by using Si nanoparticles of different diameters, as shown in Figure S4c. In each case, it was found that the maximum enhancement factor is obtained at the mirror-image-induced magnetic dipole (MMD) resonance of the Si/Au nanocavity (i.e., the plasmon mode), which appears as a scattering peak in the forward or backward scattering spectrum. For clarity, we indicated the dependence of the maximum enhancement factor on the diameter of the Si nanoparticle with a white dashed curve. It is expected that the strongest plasmon-exciton coupling is achieved in the Si/Au nanocavity with d = 176 nm. It is remarkable that the maximum enhancement factor increases with increasing diameter of the Si nanoparticle. Meanwhile, a redshift of the plasmon mode is also observed with increasing diameter of the Si nanoparticle. Therefore, it is expected that the coupling strength between the plasmons and the excitons/trions can be enhanced by shifting the exciton/trion resonance from its original position to a longer wavelength, as indicated by the white arrows. In addition, a stronger coupling strength is anticipated for the plasmons and the trions because the trions possess a longer resonance wavelength, where a larger enhancement factor is obtained. In Figure S4d,

we present the two-dimensional scattering spectra calculated for Si/WS_2/Au nanocavities composed of Si nanoparticles with different diameters at a laser power of P = 3.0 mW. One can see three scattering peaks and two scattering dips in the scattering spectra of nanocavities, which originate from strong plasmon-exciton-trion coupling induced by the laser light.

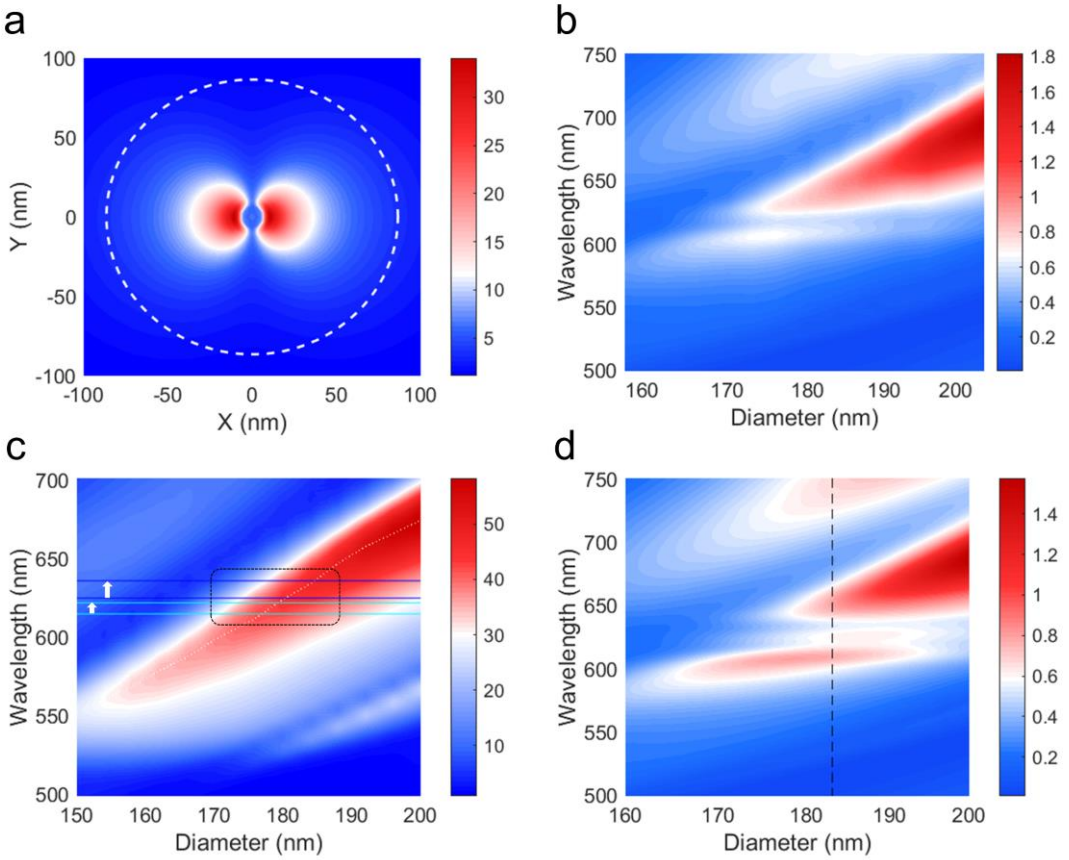

Figure S4. (a) In-plane electric field intensity distribution ($|E_{xy}/E_0|$) calculated for a Si/WS_2/Au nanocavity with d = 183 nm. (b) Two-dimensional scattering spectra calculated for Si/WS_2/Au nanocavities composed of Si nanoparticles with different diameters in the absence of the laser light. (c) In-plane electric field intensities ($|E_{xy}/E_0|^2$) calculated for Si/Au nanocavities composed of Si nanoparticles with different diameters. (d) Two-dimensional scattering spectra calculated for Si/WS_2/Au nanocavities composed of Si nanoparticles with different diameters at a laser power of P = 3.0 mW. The vertical dashed line indicates the diameter of the Si nanoparticle (d = 183 nm) in the Si/WS_2/Au nanocavity shown in (a).

Supplementary Note 7

We measured the PL spectra of Si/WS_2/Au nanocavities composed of Si nanoparticles with different diameters at different laser powers, as shown in Figure S5. In each case, the PL spectrum of the WS_2 monolayer without the Si nanoparticle obtained under the same excitation condition is also provided for comparison. It is observed that the PL spectrum in each case comprises the contributions of excitons and trions. The intensities of excitons and trions depend strongly on the laser power. The Si/WS_2/Au nanocavities can be clarified into three types based on their PL intensities. For nanocavities composed of Si nanoparticles with small diameters (a, b), the PL intensities at all laser powers are stronger than those of the WS_2 monolayer. For nanocavities built with Si nanoparticles with moderate diameters (c-f), the PL intensities at all laser powers are weaker than those of the WS_2 monolayer. For nanocavities created with Si nanoparticles with large diameters (g, h), the PL intensities are weaker or stronger than those of the WS_2 monolayer, depending on the laser power.

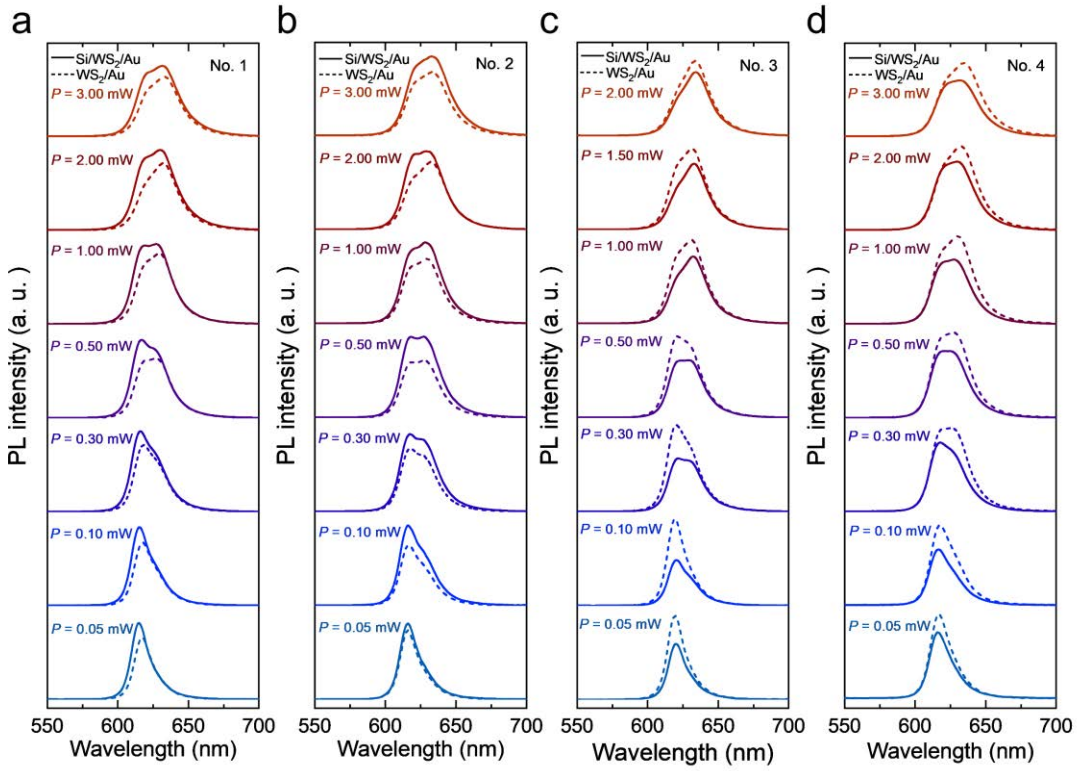

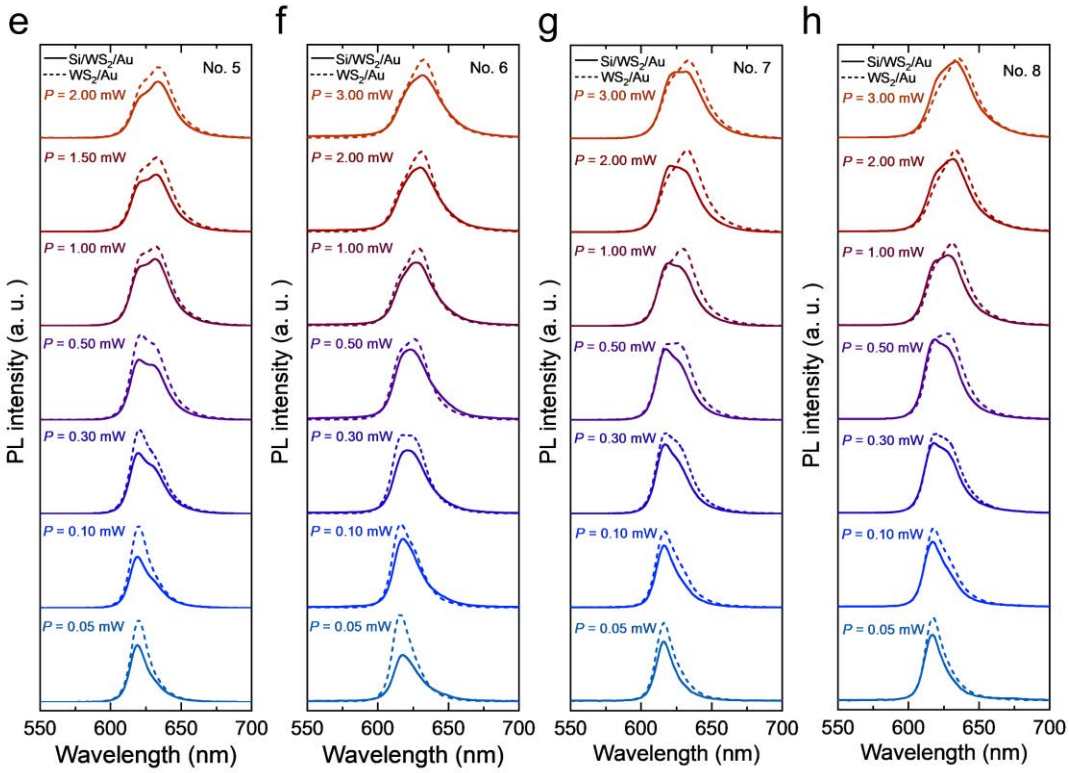

Figure S5. PL spectra measured for $Si/WS_2/Au$ nanocavities constructed with Si nanoparticles of different diameters at different laser powers. The PL spectra of the nearby WS_2 monolayer measured under the same conditions are provided for comparison.

Supplementary Note 8

As discussed in the main text, the scattering spectra of a Si/WS_2/Au nanocavity can be modified by injecting excitons/trions via the irradiation of the nanocavity with a laser beam. In this case, the modified scattering spectrum can be extracted two methods, which are described in Eqs. (3) and (5), respectively. In the first method, we first measured the scattering spectra of a nanocavity irradiated by using a laser beam with different powers. Then, we obtained the PL spectra of the nearby WS_2 monolayer (without the Si nanoparticle) at different laser powers. Finally, the modified scattering spectra can be derived by subtracting the latter spectra from the former ones. In the second method, we first measured the scattering spectra of a Si/WS_2/Au nanocavity in the absence of the laser beam. Then, we obtained the PL spectra of the nanocavity at different laser powers and those of the nearby WS_2 monolayer under the same conditions. Finally, we could extract the modified scattering spectra of the nanocavity at different laser powers based on Eq. (5). In Figure S6a, we present the modified scattering spectra derived for a nanocavities (No. 6) by using the first method. Accordingly, the modified scattering spectra extracted by using the second method are presented in Figure S6b. It is found that modified scattering spectra derived by using the two methods are exactly the same.

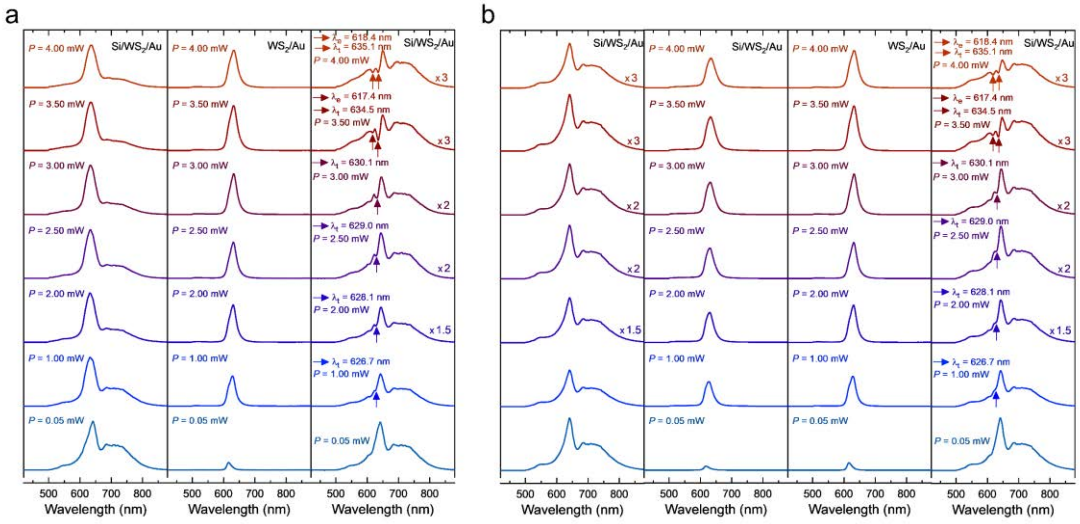

Figure S6. (a) Scattering spectra measured for a Si/WS_2/Au nanocavity (No. 6) irradiated by using laser light with different powers (first column). The PL spectra of the WS_2 monolayer measured at different laser powers and the extracted scattering spectra of the nanocavity irradiated by laser light at different powers are presented in the second and third columns, respectively. (b) Scattering spectra

measured for the nanocavity in the absence of the laser light (first column). The PL spectra of the nanocavity and the WS_2 monolayer measured at different laser powers and the extracted scattering spectra of the nanocavity irradiated by laser light at different powers are presented in the second, third and fourth columns, respectively.

Supplementary Note 9

Due to the nonuniformity of the WS_2 monolayer, there exists a fluctuation in the PL intensities measured at different positions. In Figure S7a, we show the dark-field image of a Si/WS_2/Au nanocavity. The Si nanoparticle used to construct the nanocavity is enclosed by a dashed circle. We measured the PL spectra of the WS_2 monolayer at different positions around the Si nanoparticle, as marked by solid circles. The PL spectra measured at these positions are presented in Figure S7b. In Figure S7c, we evaluate the fluctuation of the PL intensity with respect to the average value. It is noticed that the fluctuation in the PL intensity is smaller than ±10%. In Figure S7d, we present the scattering spectra derived by using PL spectra with different deviations from the average value as references. Except the change in the scattering intensity, the positions of the scattering peaks used to extract the energies of the plexciton states remain nearly unchanged.

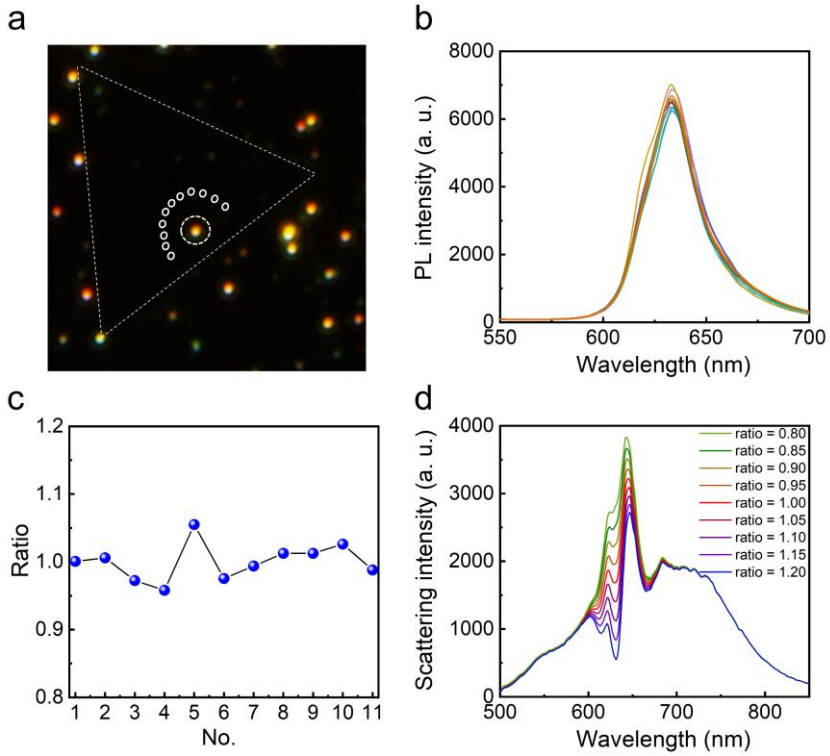

Figure S7. (a) Dark-field image of a Si/WS_2/Au nanocavity. The Si nanoparticle is enclosed by the dashed circle. The solid circles indicate the positions at which the PL spectra of the WS_2 monolayer are examined. (b) PL spectra measured for the WS_2 monolayer at different positions. (c) Fluctuation in the PL intensities measured at different positions with respect to the average value. (d) Scattering spectra of the Si/WS_2/Au nanocavity derived by using PL spectra with different deviations with respect to the average value as references.

Supplementary Note 10

In order to obtain the coupling strength (i.e., g_e and g_t) for a plasmon-exciton-trion system, we fitted the scattering spectra measured at different laser powers (see Figure S8) based on the coupled harmonic oscillator model. In each case, the scattering spectrum coincides with the fitting result except the magnetic dipole appearing at the long wavelength side of the scattering spectrum, which is not considered in the model.

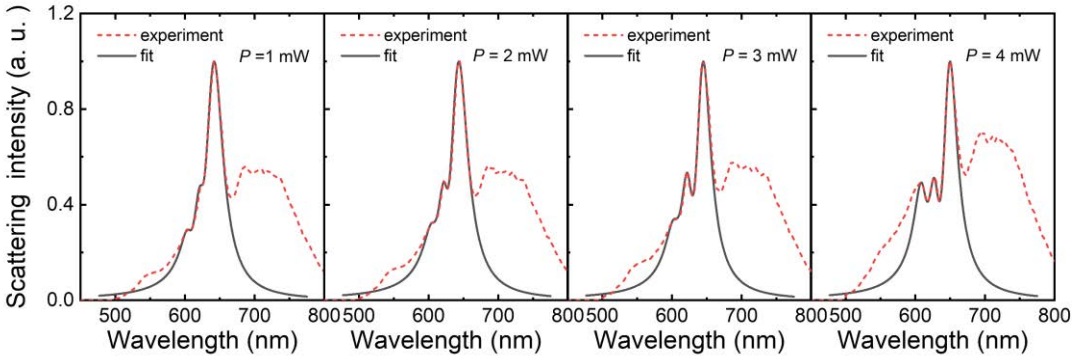

Figure S8. Scattering spectra measured for the Si/WS_2/Au nanocavity (No. 6) at different laser powers (red dashed curves) and fit results (black solid curves) based on the coupled harmonic oscillator model.

Supplementary Note 11

In Figure S9, we present the scattering spectra extracted for a Si/WS_2/Au nanocavity (No. 5) irradiated by using laser light at different laser powers. It is remarkable that a scattering dip emerges in the scattering spectrum at a laser power of P = 0.10 mW. It originates from the coupling of excitons with the nanocavity. As the laser power is raised, the Fano dip becomes deeper due to the increase in the number of injected excitons. When the laser power is increased to P = 1.50 mW, two scattering dips can be observed in the scattering spectrum owing to the plasmon-exciton-trion coupling.

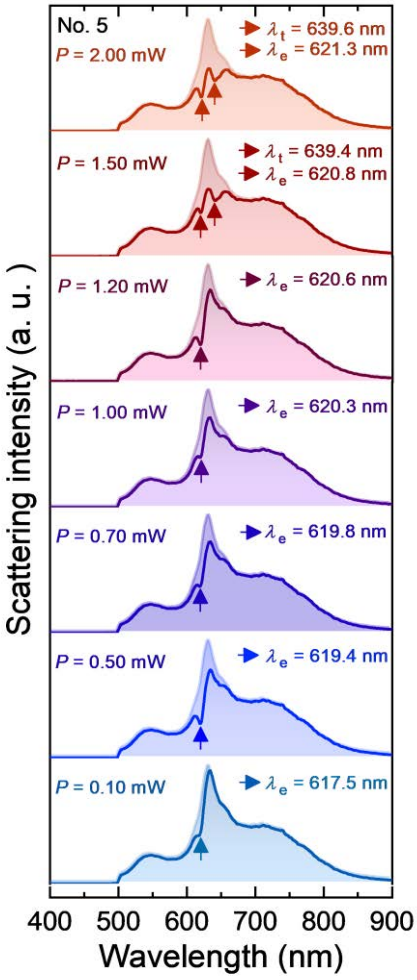

Figure S9. Scattering spectra (solid curves) derived for a Si/WS_2/Au nanocavity with d ~ 180 nm (No. 5) irradiated by using 488-nm laser light with different powers. The scattering spectra of the nanocavities in the absence of the laser light are also provided for reference (shaded graphs). The exciton and trion resonances, which appear as scattering dips in the scattering spectra, are indicated by arrows.

Supplementary Note 12

As discussed in the main text, the plasmon-exciton and plasmon-trion coupling strengths are partially determined by the in-plane electric field ($|E_{xy}/E_0|^2$) obtained in a Si/Au nanocavity at the resonant wavelengths of excitons and trions. Based on the experimental observations, the initial resonant wavelengths of excitons and trions are located at 615 and 625 nm, respectively. They are shifted to 622 and 636 nm at the largest laser power (~3.00 mW). In Figure S10a, we show the dependence of the in-plane electric field on the diameter of the Si nanoparticle. It can be seen that the strongest in-plane electric field for excitons at 615 nm is achieved in the Si/Au with d ~ 178.2 nm. In comparison, the strongest in-plane electric field for trions at 625 nm is observed in the Si//Au with d ~ 181.6 nm. With increasing laser power, an enhanced in-plane electric field is observed for excitons in nanocavities with d > 178.5 nm and a reduced electric field is expected in nanocavities with d < 178.5 nm. Similar behavior is observed for trions. In Figure S10b, we present the dependences of the in-plane electric field on the wavelength calculated for different nanocavities. From these relationships, one can easily find out the change of the in-plane electric field and its influence on the coupling strength induced by the laser irradiation, which causes the red shifts of the resonant wavelengths of excitons and trions.

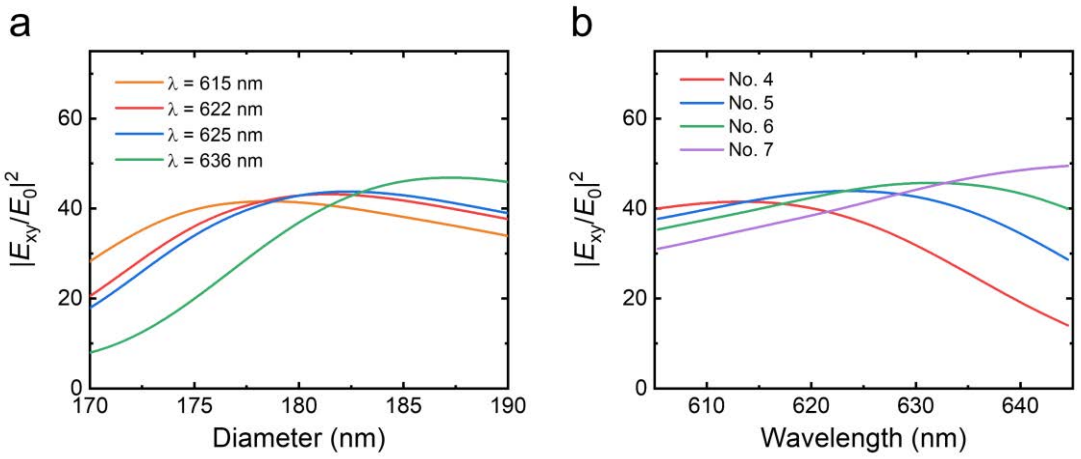

Figure S10. (a) Dependences of the in-plane electric field ($|E_{xy}/E_0|^2$) on the diameter of the Si nanoparticle obtained at different wavelengths. (b) Dependences of the in-plane electric field ($|E_{xy}/E_0|^2$) on the wavelength obtained for Si nanoparticles with different diameters.

Supplementary Note 13

The criterion for the strong coupling of three oscillators can be derived by the following formula:[10, 11]

$$\Omega > W_{UP} \cdot \gamma_{UP} + W_{MP} \cdot \gamma_{MP} + W_{LP} \cdot \gamma_{LP}. \tag{3}$$

Here, W_{UP}, W_{MP}, and W_{LP} represent the fractions of the UP, MP, and LP in the hybrid state, γ_{UP}, γ_{MP}, and γ_{LP} denote the linewidths of the UP, MP, and LP. The weights for the three branches can be derived by the following formula:

$$\begin{cases} W_{UP} = \gamma_{UP} / \left(\gamma_{UP} + \gamma_{MP} + \gamma_{LP} \right) \\ W_{MP} = \gamma_{MP} / \left(\gamma_{UP} + \gamma_{MP} + \gamma_{LP} \right) \\ W_{LP} = \gamma_{LP} / \left(\gamma_{UP} + \gamma_{MP} + \gamma_{LP} \right) \end{cases}. \tag{4}$$

In addition, the linewidths of the three branches can be obtained from the fractions of the plasmon, exciton, and trion in the hybrid states at a laser power of P = 1.00 mW (see Figure S11a):

$$\begin{cases} \gamma_{UP} = 6.95\% \gamma_{pl} + 92.35\% \gamma_{e} + 0.70\% \gamma_{t} \\ \gamma_{MP} = 11.77\% \gamma_{pl} + 2.83\% \gamma_{e} + 85.40\% \gamma_{t} \\ \gamma_{LP} = 81.29\% \gamma_{pl} + 4.74\% \gamma_{e} + 13.97\% \gamma_{t} \end{cases}. \tag{5}$$

Here, we have γ_{pl} = 106 meV, γ_{e} = 56 meV, γ_{t} = 48 meV for a nanocavity (No. 6) at P = 1.00 mW. By substituting Eqs. (5) and (4) into Eq. (3), we can derive the criterion for the strong coupling of plasmon-exciton-trion as follows:

$$\Omega > 42.03\% \gamma_{pl} + 29.03\% \gamma_{e} + 28.94\% \gamma_{t}. \tag{6}$$

Obviously, the strong-coupling criterion is fulfilled at a laser power above P = 1.00 mW (in Figure S11b).

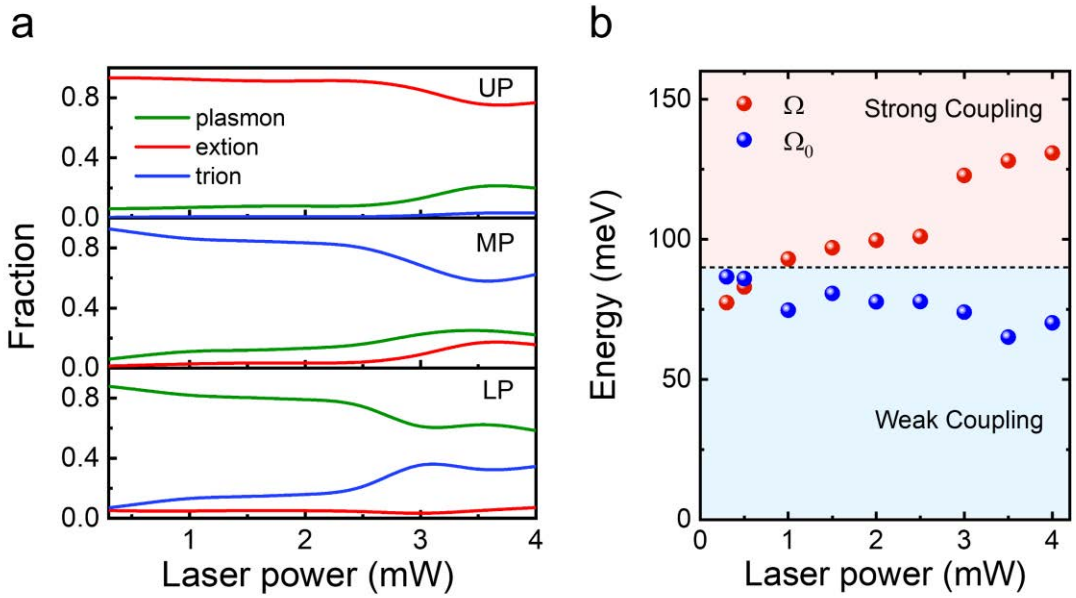

Figure S11. (a) Hopfield coefficients derived for the plasmon, exciton, and trion in the upper, middle, and lower plexcitons as a function of laser power for a Si/WS_2/Au nanocavity (No. 6). (b) Dependences of the Rabi splitting energy (i.e., Ω) (red symbols) and critical splitting energy (i.e., $Ω_0$) (blue symbols) for strong coupling on the laser power.

Supplementary Note 14

The experimental setup used for optical characterization is schematically shown in Figure S12. In our experiments, we measured the laser power at the entrance of the microscope so that the laser power can be easily adjusted. We have examined the laser power coming out of the objective and found an attenuation factor of ~0.40. It means that the actual laser power should be multiplied by a factor of 0.40.

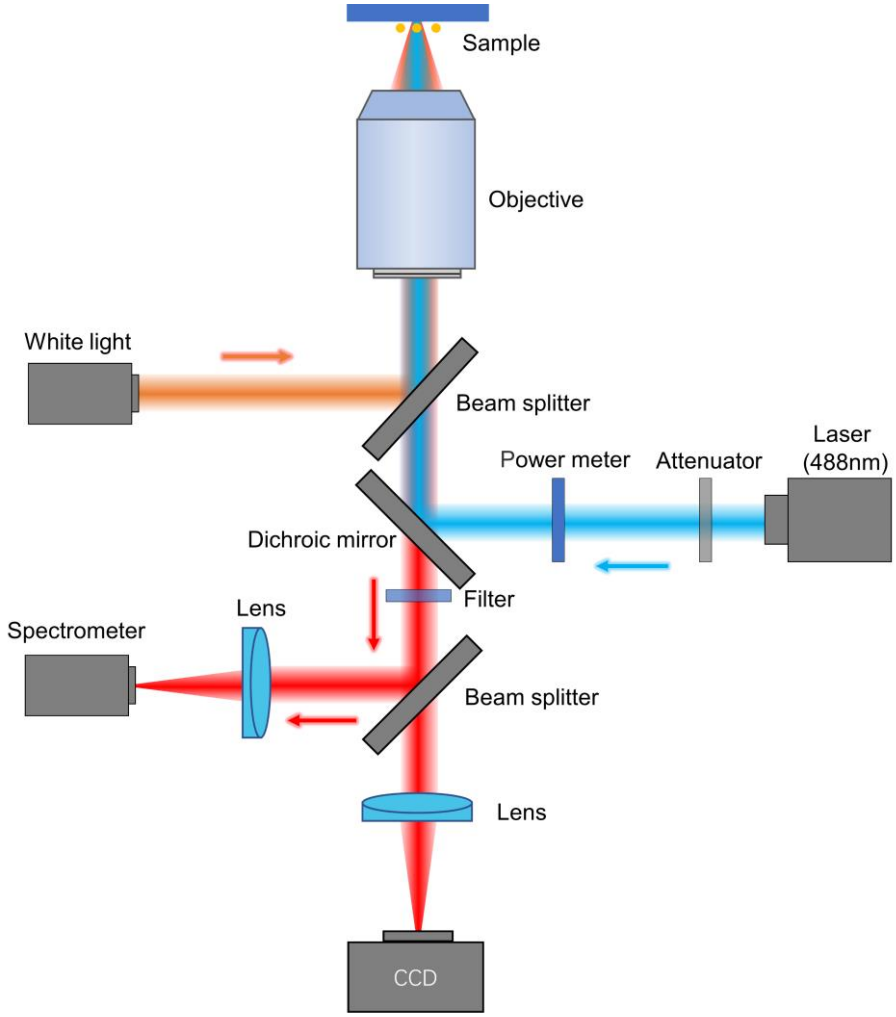

Figure S12. Schematic showing the experimental setup used to measure the PL and scattering spectra of Si/WS_2/Au nanocavities.

References

(1) Peng, B.; Zhang, H.; Shao, H.; Xu, Y.; Zhang, X.; Zhu, H. Thermal Conductivity of Monolayer MoS_2, $MoSe_2$, and WS_2: Interplay of Mass Effect, Interatomic Bonding and Anharmonicity. *RSC Adv.* **2016**, *6*, 5767–5773.

(2) Han, D.; Sun, H.; Ding, W.; Chen, Y.; Wang, X.; Cheng, L. Effect of Biaxial Strain on Thermal Transport in WS_2 Monolayer from First Principles Calculations. *Phys. E* **2020**, *124*, 114312.

(3) Zengin, G.; Wersall, M.; Nilsson, S.; Antosiewicz, T. J.; Kall, M.; Shegai, T. Realizing Strong Light-Matter Interactions between Single-Nanoparticle Plasmons and Molecular Excitons at Ambient Conditions. *Phys. Rev. Lett.* **2015**, *114*, 157401.

(4) Reithmaier, J. P.; Sek, G.; Loffler, A.; Hofmann, C.; Kuhn, S.; Reitzenstein, S.; Keldysh, L. V.; Kulakovskii, V. D.; Reinecke, T. L.; Forchel, A. Strong Coupling in a Single Quantum Dot-Semiconductor Microcavity System. *Nature* **2004**, *432*, 197–200.

(5) Chikkaraddy, R.; de Nijs, B.; Benz, F.; Barrow, S. J.; Scherman, O. A.; Rosta, E.; Demetriadou, A.; Fox, P.; Hess, O.; Baumberg, J. J. Single-Molecule Strong Coupling at Room Temperature in Plasmonic Nanocavities. *Nature* **2016**, *535*, 127–130.

(6) Huang, S.; Ming, T.; Lin, Y.; Ling, X.; Ruan, Q.; Palacios, T.; Wang, J.; Dresselhaus, M.; Kong, J. Ultrasmall Mode Volumes in Plasmonic Cavities of Nanoparticle-on-Mirror Structures. *Small* **2016**, *12*, 5190–5199.

(7) Huang, H.; Deng, F.; Xiang, J.; Li, S.; Lan, S. Plasmon-Exciton Coupling in Dielectric-Metal Hybrid Nanocavities with an Embedded Two-Dimensional Material. *Appl. Surf. Sci.* **2021**, *542*, 148660.

(8) Li, Y. Measurement of the Optical Dielectric Function of Monolayer Transition Metal Dichalcogenides: MoS_2, $MoSe_2$, WS_2, and WSe_2. In *Probing the Response of Two-Dimensional Crystals by Optical Spectroscopy*; Springer Cham: 2016; pp 33–43.

(9) Palummo, M.; Bernardi, M.; Grossman, J. C. Exciton Radiative Lifetimes in Two-Dimensional Transition Metal Dichalcogenides. *Nano Lett.* **2015**, *15*, 2794–2800.

(10) Li, B.; Zu, S.; Zhang, Z.; Zheng, L.; Jiang, Q.; Du, B.; Luo, Y.; Gong, Y.; Zhang, Y.; Lin, F.; Shen, B.; Zhu, X.; Ajayan, P. M.; Fang, Z. Large Rabi Splitting Obtained in Ag-WS_2 Strong-Coupling Heterostructure with Optical Microcavity at Room Temperature. *Opto-Electron. Adv.* **2019**, *2*, 190008.

(11) Deng, F.; Huang, H.; Chen, J. D.; Liu, S.; Pang, H.; He, X.; Lan, S. Greatly Enhanced Plasmon-Exciton Coupling in Si/WS_2/Au Nanocavities. *Nano Lett.* **2022**, *22*, 220–228.